Parameterisation of injection-dependent lifetime measurements in semiconductors in terms of Shockley-Read-Hall statistics: An application to oxide precipitates in silicon

J. D. Murphy,[1,a)] K. Bothe,[2] R. Krain,[2] V. V. Voronkov,[3] and R. J. Falster[1,3]
[1]*Department of Materials, University of Oxford, Parks Road, Oxford OX1 3PH, United Kingdom*
[2]*Institut für Solarenergieforschung Hameln/Emmerthal, Am Ohrberg 1, 31860 Emmerthal, Germany*
[3]*MEMC Electronic Materials, via Nazionale 59, 39012 Merano, Italy*

(Received 26 March 2012; accepted 3 May 2012; published online 7 June 2012)

Injection-dependent minority carrier lifetime measurements are a valuable characterisation method for semiconductor materials, particularly those for photovoltaic applications. For a sample containing defects which obey Shockley-Read-Hall statistics, it is possible to use such measurements to determine (i) the location of energy levels within the band-gap and (ii) the ratios of the capture coefficients for electrons and holes. In this paper, we discuss a convenient methodology for determining these parameters from lifetime data. Minority carrier lifetime is expressed as a linear function of the ratio of the total electron concentration to the total hole concentration for p-type (or vice versa for n-type) material. When this is plotted on linear scales, a single-level Shockley-Read-Hall centre manifests itself as a straight line. The gradient and intercepts of such a plot can be used to determine recombination parameters. The formulation is particularly instructive when multiple states are recombination-active in a sample. To illustrate this, we consider oxide precipitates in silicon as a case study and analyse lifetime data for a wide variety of p-type and n-type samples as a function of temperature. We fit the data using both a single two-level defect and two independent single-level defects and find the latter can fit the lifetime curves in all cases studied. The first defect is at $E_V + 0.22\,eV$ and has a capture coefficient for electrons ~157 times greater than that for holes at room temperature. The second defect is at $E_C - 0.08\,eV$ and has a capture coefficient for holes ~1200 times greater than that for electrons at room temperature. We find that the presence of dislocations and stacking faults around the precipitates acts to increase the density of both states without introducing new levels. Using the analysis method described, we present a parameterisation of the minority carrier lifetime in silicon containing oxide precipitates. © *2012 American Institute of Physics*. [http://dx.doi.org/10.1063/1.4725475]

I. INTRODUCTION

Minority carrier lifetime is an important figure of merit in semiconductor materials, particularly those used for photovoltaics as lifetime critically affects solar cell energy conversion efficiency. Shockley-Read-Hall (SRH) statistics are used to quantify recombination of charge carriers at many defects in semiconductors.[1,2] Temperature- and injection-dependent lifetime spectroscopy (TIDLS) measurements can be used to determine approximate energy levels and the ratios of the capture coefficients for electrons to those of holes.[3–5] Early attempts at developing injection-level analysis were made in the 1992 to 1995 European ESPRIT project "DIASYSCON," which aimed to study sub-parts per trillion levels of contamination in silicon for microelectronic applications (some results are presented in Ref. 6). The later development of the quasi-steady-state photoconductance (QSS-PC) technique[7] now means that TIDLS is routinely used to characterise silicon photovoltaic materials. TIDLS enables defects present in concentrations well below the detection limit of deep-level transient spectroscopy (DLTS)[8] to be studied.[3]

Czochralski silicon (Cz-Si) typically contains up to $\sim 10^{18}\,cm^{-3}$ of interstitial oxygen. In Cz-Si for integrated circuits, thermal processing is routinely used to create controlled distributions of oxide precipitates. Such defects also form unintentionally in both Cz-Si and multicrystalline silicon (mc-Si) for solar cells.[9,10] Oxide precipitates can be extremely beneficial because they getter device-ruining metallic contaminants.[11,12] It has recently been suggested that oxygen precipitation lies at the heart of the mechanism for gettering in highly phosphorus doped emitter regions formed during most silicon solar cell production processes.[13] Oxide precipitates can also affect the mechanical stability of wafers at elevated temperatures[14,15] and can alter the mechanism of room temperature wafer fracture.[16] Oxide precipitates and surrounding defects act as recombination centres[17–25] and this can cause a reduction in solar cell efficiencies.[10,26] It is important to understand the mechanism by which recombination occurs at the precipitates and to be able to quantify their effect on minority carrier lifetime.

Studying recombination associated with oxide precipitates is not straightforward. The morphology of the precipitates evolves during growth from an unstrained to a strained state, and strained precipitates can be surrounded by dislocations and stacking faults.[27,28] Our recent work using photoconductance methods on p-type Cz-Si shows that the recombination rate at a given injection level varies approximately linearly with the density of strained precipitates.[24]

a)E-mail: john.murphy@materials.ox.ac.uk.

This relationship was confirmed by an electrically detected magnetic resonance (EDMR) study on the same sample set.[25] The rate of recombination was also found to be higher when dislocations and stacking faults surrounded the precipitates.[24]

Voronkov *et al*. have recently introduced a formulation of SRH statistics which allows SRH parameters easily to be extracted from TIDLS data.[29,30] This has been particularly valuable in studying the boron-oxygen defect responsible for light-induced degradation of silicon solar cells.[29,30] We begin this paper by describing this analysis approach, showing how SRH parameters can be determined by using it. We then apply the framework to improve the understanding of recombination at oxide precipitates in silicon. We extend our previous room temperature study on p-type material[24] to include n-type specimens of different resistivities and temperature-dependent measurements. We find that recombination at oxide precipitates can be parameterised in terms of just two independent SRH centres. SRH parameters are determined which enable the effect of oxide precipitates on minority carrier lifetime in silicon to be quantitatively determined.

II. ANALYSIS OF LIFETIME DATA IN TERMS OF SRH STATISTICS

A. Linear formulation of SRH statistics

The net recombination rate of carriers in a semiconductor, R, can be determined by finding the difference between the capture and emission of carriers from a recombination centre. By considering the statistics of two charge states of a one-level recombination centre, it can be shown that[1,2]

$$R = \frac{(np - n_i^2)\alpha_n\alpha_p N}{\alpha_n(n+n_1) + \alpha_p(p+p_1)}, \tag{1}$$

where n is the electron concentration, p is the hole concentration, n_i is the intrinsic carrier concentration, α_n is the recombination centre's capture coefficient for electrons, α_p is the recombination centre's capture coefficient for holes and N is the density of the recombination centre. Capture coefficients are the product of the thermal velocity and the capture cross-section. The SRH densities, n_1 and p_1, are defined according to

$$n_1 = N_C \exp\left(-\frac{(E_C - E_T)}{k\mathrm{T}}\right), \tag{2}$$

$$p_1 = N_V \exp\left(-\frac{(E_T - E_V)}{k\mathrm{T}}\right), \tag{3}$$

where N_C and N_V are the density of states in the conduction and valence bands respectively, and E_T is the energy level of the defect.

The electron concentration is given by $n = n_0 + \Delta n$, where n_0 is the equilibrium electron concentration and Δn is the excess electron concentration. The hole concentration is given by $p = p_0 + \Delta p$, where p_0 is the equilibrium hole concentration and Δp is the excess hole concentration. The use of these expressions together with the law of mass action gives the following general expression for recombination rate at a one-level centre:

$$R = \frac{(n_0\Delta p + p_0\Delta n + \Delta n\Delta p)\alpha_n\alpha_p N}{\alpha_n(n+n_1) + \alpha_p(p+p_1)}. \tag{4}$$

Equation (4) simplifies when the type of material is known. In p-type material $\mathrm{p_0} \gg \mathrm{n_0}$, so $n_0\Delta p$ is negligible and, to a very good approximation, the bracketed term in the numerator of Eq. (4) is $p\Delta n$. The electron lifetime is given by $\tau_n = \frac{\Delta n}{R}$, which using Eq. (4) becomes

$$\tau_n = \frac{1}{\alpha_n N}\left(\frac{Q(n+n_1)}{p} + 1 + \frac{p_1}{p}\right), \tag{5}$$

where $Q = \frac{\alpha_n}{\alpha_p}$. The increment in the hole concentration Δp is equal to $\Delta n + \Delta n_\mathrm{t}$ where Δn_t is the increment in the concentration of electrons trapped by the centre; the latter quantity is less than the defect concentration N. Provided $N \ll p_0$, p is identical to $p_0 + \Delta n$. As n_0 is negligible and $n \approx \Delta n$ the hole concentration is given by $p = p_0 + n$. We can, therefore, write

$$p = \frac{p_0}{1 - X}, \tag{6}$$

where $X = \frac{n}{p} = \frac{n}{p_0+n}$. Inserting Eq. (6) into Eq. (5) gives the electron lifetime in p-type material to be

$$\tau_n = \frac{1}{\alpha_n N}\left[1 + \frac{Qn_1}{p_0} + \frac{p_1}{p_0} + X\left(Q - \frac{Qn_1}{p_0} - \frac{p_1}{p_0}\right)\right]. \tag{7}$$

Similarly, it can also be shown that the hole lifetime in n-type material, τ_p, is

$$\tau_p = \frac{1}{\alpha_p N}\left[1 + \frac{n_1}{n_0} + \frac{p_1}{n_0 Q} + Y\left(\frac{1}{Q} - \frac{n_1}{n_0} - \frac{p_1}{Qn_0}\right)\right], \tag{8}$$

where $Y = \frac{p}{n} = \frac{p}{n_0+p}$.

In the Appendix, we derive expressions for the lifetime for a two-level centre as a function of n/p (for p-type) and p/n (for n-type).

B. Determination of SRH parameters from injection-dependent lifetime data

We now consider how to extract unknown parameters using this formulation of SRH statistics in the case of independent defects in p-type material. The first step is to plot the minority carrier lifetime as a function of $X = \frac{n}{p}$, correcting for any well-understood recombination mechanisms (e.g., Coulomb-enhanced Auger recombination, band-to-band recombination). If one single-level centre is active, then the plot will be linear. If multiple independent centres operate, then the data can be fitted using multiple straight lines which are combined in reciprocal to reproduce the experimentally determined data. For each centre, the line's gradient ($\frac{d\tau_n}{\mathrm{dX}}$), value as $\mathrm{X} \to 0$ ($\tau_{nX\to0}$) and value as $\mathrm{X} \to 1$ ($\tau_{nX\to1}$) can be determined. Information on the SRH parameters can be derived from these quantities, as follows. First, the $\mathrm{X} \to 1$

limit of Eq. (7) gives the so-called ambipolar lifetime—a quantity which is independent of the energy level of the defect

$$\tau_{nX\to 1} = \frac{1+Q}{\alpha_n N} = \frac{\frac{1}{\alpha_n}+\frac{1}{\alpha_p}}{N}. \quad (9)$$

Second, dividing the gradient by the X → 1 limit gives a quantity which is independent of the centre concentration. From Eqs. (7) and (9)

$$\frac{d\tau_n}{\mathrm{dX}} \Big/ \tau_{nX\to 1} = \frac{Q}{1+Q} - \frac{1}{p_0}\left(\frac{Qn_1+p_1}{1+Q}\right). \quad (10)$$

Plotting this quantity versus the reciprocal of the doping level, $\frac{1}{p_0}$, allows Q to be determined from the intercept and $Qn_1 + p_1$ to be determined from the gradient. Third, the X → 0 limit of Eq. (7) is

$$\tau_{nX\to 0} = \frac{1}{\alpha_n N}\left[1+\frac{1}{p_0}(Qn_1+p_1)\right]. \quad (11)$$

This allows the determination of the $\alpha_n N$ parameter, either from a plot of $\tau_{nX\to 0}$ against $\frac{1}{p_0}$ or from substitution of $Qn_1 + p_1$ found from Eq. (9) and a single doping level.

Equations equivalent to Eqs. (9)–(11) for n-type silicon can be, respectively, derived as

$$\tau_{pY\to 1} = \frac{1+Q}{\alpha_n N} = \frac{\frac{1}{\alpha_n}+\frac{1}{\alpha_p}}{N}, \quad (12)$$

$$\frac{d\tau_p}{\mathrm{dY}} \Big/ \tau_{pY\to 1} = \frac{1}{1+Q} - \frac{1}{n_0}\left(\frac{n_1+\frac{p_1}{Q}}{1+Q}\right), \quad (13)$$

$$\tau_{pY\to 0} = \frac{1}{\alpha_p N}\left[1+\frac{1}{n_0}\left(n_1+\frac{p_1}{Q}\right)\right]. \quad (14)$$

In practice, there are three simplifying cases due to different possible locations of the trap level in the bandgap (E_G). For a deep defect ($E_T \to E_G/2$), n_1 and p_1 terms in the above equations are negligible. In this case, the only temperature-dependence of the lifetime arises from the temperature-dependence of the capture coefficients. For a level close to the valence band ($E_T \to E_V$) n_1 terms are negligible, and for a level close to the conduction band ($E_T \to E_C$) p_1 terms are negligible. In this paper, Eqs. (9)–(14) are used to extract SRH parameters for recombination at oxide precipitates in silicon.

III. EXPERIMENTAL METHODS FOR LIFETIME TESTING

A. Samples

Experiments were conducted on both p-type and n-type samples. Most p-type samples were doped with $\sim 1\times10^{15}\,\mathrm{cm^{-3}}$ of boron and had an initial oxygen concentration of $7.7\times10^{17}\,\mathrm{cm^{-3}}$ (DIN50438/I (1995)). To form the oxide precipitates, the 150 mm diameter wafers were subjected to a four-stage thermal treatment described in detail elsewhere.[24,31] A range of nucleation and growth conditions were used to create a matrix of samples with a wide range of precipitate concentrations and morphologies. Strained precipitate densities ($N_{strained}$) were measured by Schimmel etching and densities ranged from $3\times10^{6}\,\mathrm{cm^{-3}}$ to $7\times10^{10}\,\mathrm{cm^{-3}}$. To investigate the doping dependence of the recombination process, p-type samples with doping levels ranging from $3.9\times10^{14}\,\mathrm{cm^{-3}}$ to $8.2\times10^{15}\,\mathrm{cm^{-3}}$ were also studied. These had a wide range of initial oxygen concentrations (5.9 to $9.6\times10^{17}\,\mathrm{cm^{-3}}$) but were processed under different conditions to give a narrow range of strained precipitate densities (2.0 to $2.9\times10^{10}\,\mathrm{cm^{-3}}$). The n-type samples were doped with phosphorus and two samples were selected from each of three 200 mm diameter ingots. Samples from "Ingot 1" had a doping level of $9\times10^{14}\,\mathrm{cm^{-3}}$ to $1.0\times10^{15}\,\mathrm{cm^{-3}}$ and an initial oxygen concentration of $8.5\times10^{17}\,\mathrm{cm^{-3}}$. They were processed using similar conditions to the p-type samples to give strained oxide precipitate densities of $1.1\times10^{10}\,\mathrm{cm^{-3}}$ and $1.4\times10^{14}\,\mathrm{cm^{-3}}$. Samples from "Ingot 2" had a doping level of $6\times10^{13}\,\mathrm{cm^{-3}}$ to $9\times10^{13}\,\mathrm{cm^{-3}}$ and an initial oxygen concentration of $6.5\times10^{17}\,\mathrm{cm^{-3}}$. They were subjected to a modified thermal process, which included a 4 h anneal at 925 °C before the growth stage to ensure all unstrained precipitates were converted to strained ones. The strained oxide precipitate densities in these samples were $2.1\times10^{10}\,\mathrm{cm^{-3}}$ and $2.6\times10^{10}\,\mathrm{cm^{-3}}$. Samples from "Ingot 3" had a doping level of $5\times10^{13}\,\mathrm{cm^{-3}}$ and an initial oxygen concentration of $5.2\times10^{17}\,\mathrm{cm^{-3}}$. They were also subjected to the modified precipitation process and contained $6.0\times10^{8}\,\mathrm{cm^{-3}}$ and $2.4\times10^{9}\,\mathrm{cm^{-3}}$ of strained oxide precipitates.

The p-type samples have also been characterised by transmission electron microscopy (TEM) and the results are discussed in more detail elsewhere.[24,28] As far as this present paper is concerned, TEM enabled the identification of samples in which some of the precipitates are surrounded by other extended defects (dislocations and stacking faults). These are known to have different recombination properties[24] and hence are treated separately.

B. Surface passivation and lifetime measurements

The surfaces of samples measuring 5 cm by 5 cm were passivated with silicon nitride deposited by plasma enhanced chemical vapour deposition (PECVD). Remote PECVD was used for the vast majority of samples, and the scheme used has previously been shown to give a surface recombination velocity below 10 cm/s.[32] Lower quality direct PECVD was used for the p-type samples set with the range of doping levels. The difference is not believed to be significant as the samples concerned had a relatively low bulk lifetime due to the high concentration of precipitates, so effects due to increased surface recombination are negligible. Room temperature minority carrier lifetime was measured using photoconductance methods[7] using a Sinton WCT-120 lifetime tester at the University of Oxford. A Sinton lifetime tester at ISFH was used for temperature-dependent measurements and the set-up used is described in Ref. 5. Temperature-dependent measurements were made from room temperature to up to 150 °C and a correction to account for the change in carrier conductivity with temperature was applied. P-type

samples were subjected to a 10 min pre-anneal at 200 °C to ensure the dissociation of boron-oxygen defects[33] and to many close-up flashes immediately before lifetime measurement to dissociate iron-boron pairs.[34,35] For temperature-dependent measurements on p-type samples, the dissociation process was repeated prior to each measurement. For room temperature measurement, a second measurement was made more than 24 h later from which bulk iron concentrations were determined using methods described in Refs. 24 and 36. Bulk iron concentrations for p-type samples were $<4\times10^{11}\,\mathrm{cm}^{-3}$, as plotted in Ref. 24. It is noted that the aggregated illumination time of the flashes of light used to dissociate the iron-boron pairs is very short (<20 ms). This is considerably shorter than the time required to form boron-oxygen defects (typically of the order of hours[33]).

IV. EXPERIMENTAL LIFETIME TESTING RESULTS

The measured minority carrier lifetime ($\tau_{measured}$) includes contributions from processes other than recombination at oxide precipitates and any surrounding defects. Some of these other recombination processes are well understood and corrections to the measured lifetime can be made to account for them. We therefore present our data in terms of a residual lifetime ($\tau_{residual}$) defined according to

$$\frac{1}{\tau_{residual}}=\frac{1}{\tau_{measured}}-\left(\frac{1}{\tau_{band-to-band}}+\frac{1}{\tau_{CE\ Auger}}+\frac{1}{\tau_{Fe_i}}\right), \tag{15}$$

where $\tau_{band\text{-}to\text{-}band}$ is the lifetime due to band-to-band recombination,[37] $\tau_{CE\ Auger}$ is the lifetime due to Coloumb-enhanced Auger recombination,[38] and τ_{Fe_i} is the lifetime due to SRH recombination at bulk interstitial iron.[35] Details of these corrections are given in our previous paper.[24] In n-type silicon, it is not possible to measure the interstitial iron concentration, so no correction is made for bulk iron-related recombination in n-type samples. These three corrections are generally small compared to the measured lifetime for samples with high concentrations of strained precipitates. However, for samples with higher measured lifetimes, the corrections can be significant, particularly at higher injection levels where Coloumb-enhanced Auger recombination becomes non-negligible.

Figure 1 shows $\tau_{residual}$ against the excess carrier density (Δp) normalised by the donor concentration (n_0) measured at room temperature in selected n-type oxide precipitate-containing samples. The lifetime measured and its injection response appears to be dependent upon both the strained precipitate density and the doping level. The room temperature injection-level dependent residual lifetime for 26 p-type oxide precipitate-containing samples has been reported previously.[24] These p-type data were from specimens with the same approximate doping levels. At a particular injection level ($0.5p_0$), the recombination rate in the p-type samples was found to be approximately dependent upon the density of the strained precipitates, with increased recombination in specimens in which dislocations and/or stacking faults surrounded the precipitates. Lifetime curves for p-type samples with different doping levels (not shown) have the same general features as the p-type

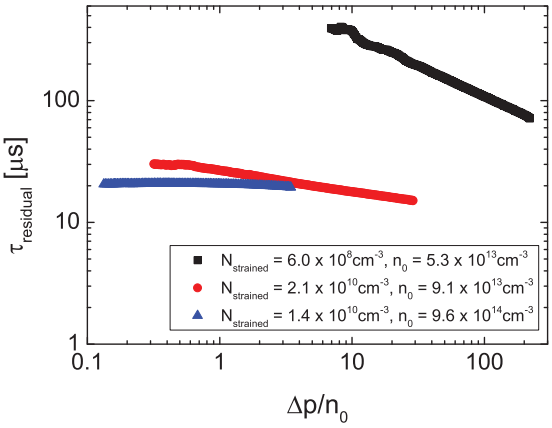

FIG. 1. Residual minority carrier lifetime measured at room temperature versus injection level for selected n-type silicon samples processed to contain oxide precipitates. The sample with a strained precipitate concentration of $1.4\times10^{10}\,\mathrm{cm}^{-3}$ was from Ingot 1, that with $2.1\times10^{10}\,\mathrm{cm}^{-3}$ was from Ingot 2, and that with $6.0\times10^{8}\,\mathrm{cm}^{-3}$ was from Ingot 3.

curves reported previously[24] with variation arising as expected from the change in doping.

Figure 2 shows the normalised residual lifetime in oxide precipitate-containing n-type samples as a function of measurement temperature. The data are from two samples with different doping levels. Figure 3 shows the residual lifetime normalised by the acceptor concentration (p_0) at different temperatures for a p-type silicon sample. The residual lifetime increases with measurement temperature in all precipitate-containing samples studied.

V. ANALYSIS OF RECOMBINATION AT OXIDE PRECIPITATES IN TERMS OF SRH STATISTICS

The lifetime curves obtained, such as those in Figures 1–3 and in our previous publication,[24] demonstrate that the residual lifetime in samples processed to contain oxide precipitates depends upon injection level, type, doping, strained oxide precipitate density, and temperature. We now use the formulation of SRH recombination described in Sec. II and

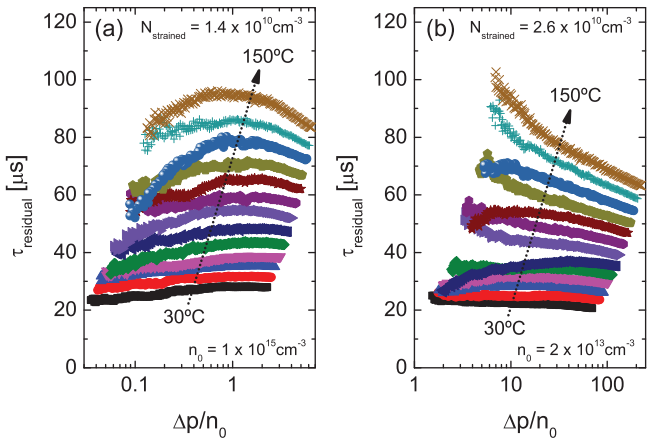

FIG. 2. Residual minority carrier lifetime versus excess carrier density normalised by the doping level in n-type silicon processed to contain oxide precipitates. Data in graph (a) are from a sample from Ingot 1. Data in graph (b) are from a sample from Ingot 2. The measurements were made from 30 °C to 150 °C in increments of 10 °C.

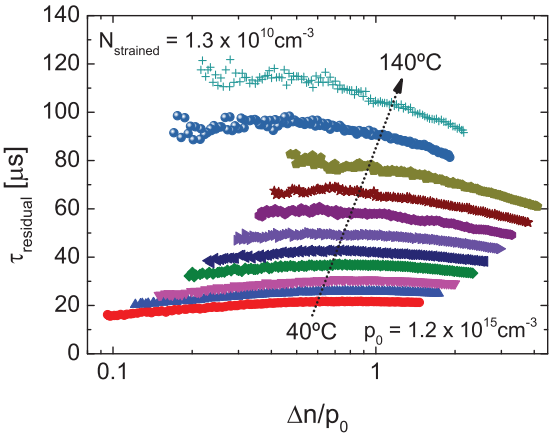

FIG. 3. Residual minority carrier lifetime versus injection level in a p-type silicon sample processed with a 16 h nucleation and 8 h growth to contain strained oxide precipitates. The measurements were made from 40 °C to 140 °C in increments of 10 °C.

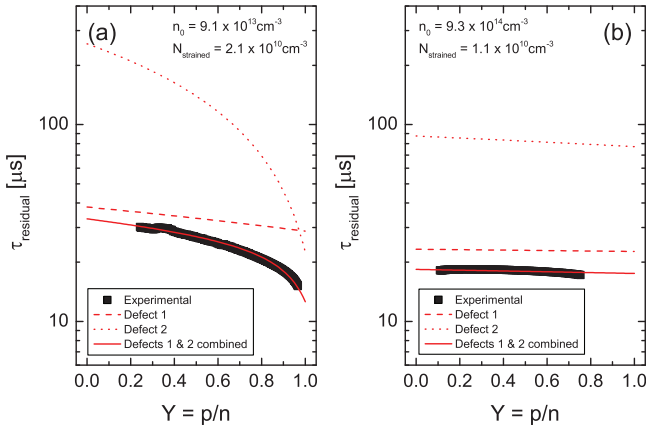

FIG. 5. Residual minority carrier lifetime versus *p*/*n* for typical n-type samples from (a) Ingot 2 and (b) Ingot 1.

the Appendix to parameterise these data in terms of SRH statistics.

A. Room temperature data

Figure 4 shows room temperature residual lifetime in p-type samples plotted against *n*/*p*. Oxide precipitates have been found to be surrounded by dislocations and stacking faults for one of these plots but not the other. Similar curves were obtained for all the other p-type samples studied. The dependence of $\tau_{residual}$ on *n*/*p* is similar in all cases. The overall non-linearity means the recombination cannot be accounted for by one single-level SRH centre described by Eq. (7). Figure 5 shows room temperature residual lifetime in n-type samples plotted against *p*/*n* for samples with different doping levels. Again, the injection dependence cannot be explained by one single-level SRH centre.

The next level of complexity offers two possibilities. The first is that oxide precipitates introduce a single defect with two energy levels, such as is the case for the fast recombination centre responsible for light-induced degradation of silicon photovoltaics.[30] The second is that recombination occurs via two independent defects, both of which result from the existence of oxide precipitates. We have attempted to fit the lifetime data using both cases. The variation of lifetime with *n*/*p* for p-type (or *p*/*n* for n-type) in the case of a single two-level centre is derived in the Appendix. For such a defect, it is possible to fit either the p-type data or the n-type data but not both with the same energy levels. Fitting the p-type data to Eq. (A10) could be achieved with energy levels at $E_V + 0.2\,eV$ and $E_V + 0.245\,eV$; fitting the n-type data to Eq. (A11) could be achieved with a negative-U centre with levels at $E_C - 0.21\,eV$ and $E_V + 0.28\,eV$. We therefore conclude that recombination at oxide precipitates cannot be explained by a single two-level defect alone.

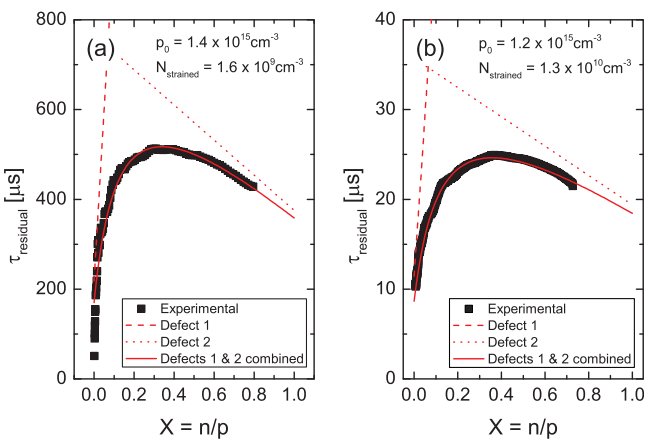

FIG. 4. Residual minority carrier lifetime versus *n*/*p* for typical p-type samples. Graph (a) is for a sample processed with an 8 h nucleation and 4 h growth to contain oxide precipitates not surrounded by other extended defects such as dislocations and stacking faults. Graph (b) is for a sample processed with a 16 h nucleation and 8 h growth to contain oxide precipitates surrounded by dislocations and stacking faults.

We next turn our attention to the case of two independent SRH centres. In Sec. II B, we describe how the SRH parameters for single-level defects can be extracted using the linear formulation of SRH statistics. All the lifetime curves obtained can be fitted by adding two independent single-level centres in reciprocal. This is shown in Figures 4 and 5 and we refer to the centres as "Defect 1" and "Defect 2." For each sample, two straight lines have been chosen to best fit the experimental data when combined in reciprocal. Figure 6 shows plots of the gradients of such lines normalised by their value as X or Y → 1 against the reciprocal of doping level. Applying Eq. (10) to the p-type data gives the ratio of the capture coefficient for electrons to that of holes for Defect 1, Q_1, as 157. The ratio of the capture coefficient for holes to that of electrons for Defect 2, $1/Q_2$, is 1200. For Defect 1, the parameter $Q_1 n_1 + p_1$, where n_1 and p_1 are the characteristic concentrations for the centre given by Eqs. (2) and (3) respectively, is $4.8 \times 10^{15}\,cm^{-3}$. For Defect 2, the parameter $Q_2 n_2 + p_2$, where n_2 and p_2 are the characteristic concentrations for the centre given by Eqs. (2) and (3) respectively, is $1.0 \times 10^{15}\,cm^{-3}$. Applying Eq. (13) to the n-type data gives the same values of Q_1 and Q_2. The value of $n_1 + \frac{p_1}{Q_1}$ is $3.1 \times 10^{13}\,cm^{-3}$ and the value of $n_2 + \frac{p_2}{Q_2}$ is $1.3 \times 10^{18}\,cm^{-3}$. The parameters deduced from p-type and n-type data are therefore in excellent agreement. Whether the energy levels of the two defects lie close to the valence or conduction band edges is determined from the temperature-dependent data in Sec. V C.

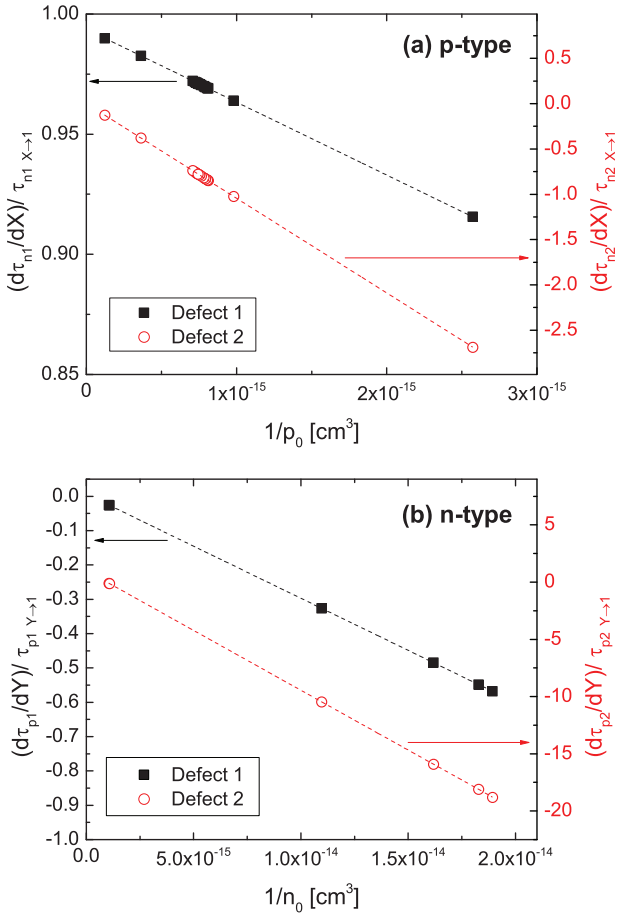

FIG. 6. The gradients of the n/p (for p-type) or p/n (for n-type) lines fitted through the experimental data normalised by the lifetime as n/p or $p/n \rightarrow 1$ plotted against the reciprocal of the doping level. Plot (a) is for p-type material according to Eq. (10). Plot (b) is for n-type material according to Eq. (13).

B. Relationship between recombination parameters and precipitate density

From lifetime measurements alone it is not possible to determine the absolute densities, N_1 and N_2, of the two independent SRH centres identified. However, it is possible to analyse the independent linear fits to the experimental data to deduce $N_1\alpha_{n1}$ and $N_2\alpha_{n2}$ from the p-type data using Eq. (11) and $N_1\alpha_{p1}$ and $N_2\alpha_{p2}$ from the n-type data using Eq. (14). The p-type parameters are plotted against the measured concentration of strained precipitates in Figure 7(a) for the case when oxide precipitates are not surrounded by dislocations and stacking faults and in Figure 7(b) in the case when the oxide precipitates are surrounded by other extended defects. In both plots, the correlation of $N_1\alpha_{n1}$ and $N_2\alpha_{n2}$ with $N_{strained}$ is approximately linear. The gradients of the best-fit lines constrained to pass through the origin are (a) 1.7×10^{-5} cm^{3}s^{-1} for $N_1\alpha_{n1}$ and 1.8×10^{-6} cm^{3}s^{-1} for $N_2\alpha_{n2}$ for samples in which oxide precipitates are not surrounded by other extended defects and (b) 2.9×10^{-5} cm^{3}s^{-1} for $N_1\alpha_{n1}$ and 5.1×10^{-6} cm^{3}s^{-1} for $N_2\alpha_{n2}$ for samples in which dislocations or stacking faults were found to surround some of the oxide precipitates. The presence of dislocations and stacking faults around the precipitates increases the gradient by a factor of ~1.7 in the case of $N_1\alpha_{n1}$ and ~2.9 in the case of $N_2\alpha_{n2}$. Approximately linear behaviour

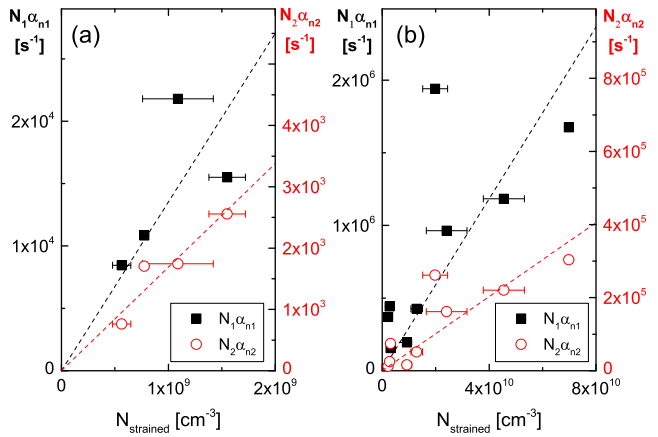

FIG. 7. Variation of the $N_1\alpha_{n1}$ and $N_2\alpha_{n2}$ fit parameters determined using Eq. (11) with the density of strained oxide precipitates, $N_{strained}$, for p-type samples in which (a) the oxide precipitates are not surrounded by dislocations or stacking faults and (b) some oxide precipitates are surrounded by dislocations or stacking faults.

is also found in n-type material, as plotted in Figure 8. In this case, the gradients are 2.7×10^{-6} cm^{3}s^{-1} for $N_1\alpha_{n1}$ and 1.6×10^{-3} cm^{3}s^{-1} for $N_2\alpha_{p2}$.

C. Temperature-dependent data

Figure 9(a) shows the residual lifetime measured at selected temperatures in a p-type sample plotted against n/p, and Figure 9(b) shows the residual lifetime measured at the same temperatures in an n-type sample plotted against p/n. The curves can all be fitted using the two independent SRH centres. Figure 10 shows the variation in the lifetime as $X \rightarrow 1$ with temperature for both defects in the p-type case. Arrhenius behaviour is found in both cases. If it is assumed that the density of defects does not change with temperature, then Eq. (9) can be used to deduce information on the temperature dependence of the capture coefficients. Defect 1 is known to have $Q \gg 1$, so consequently the activation energy of 0.20 ± 0.2 eV for the lifetime as $X \rightarrow 1$ corresponds to that of its capture coefficient for holes, α_{p1}. Defect 2 is known to have $Q \ll 1$, so the activation energy of 0.14 ± 0.02 eV is that of its capture coefficient for electrons, α_{n2}.

The temperature-dependent lifetime data can be used to determine the half of the band-gap in which the energy levels

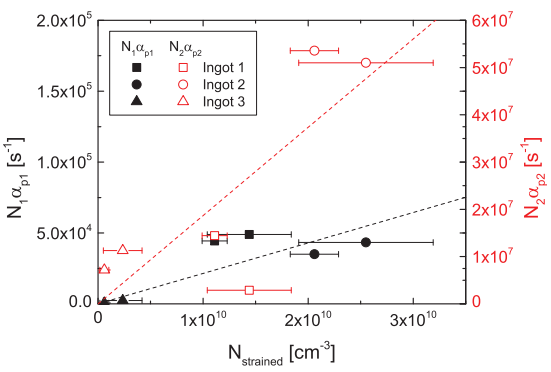

FIG. 8. Variation of the $N_1\alpha_{p1}$ and $N_2\alpha_{p2}$ fit parameters determined using Eq. (14) with the density of strained oxide precipitates, $N_{strained}$, for n-type samples.

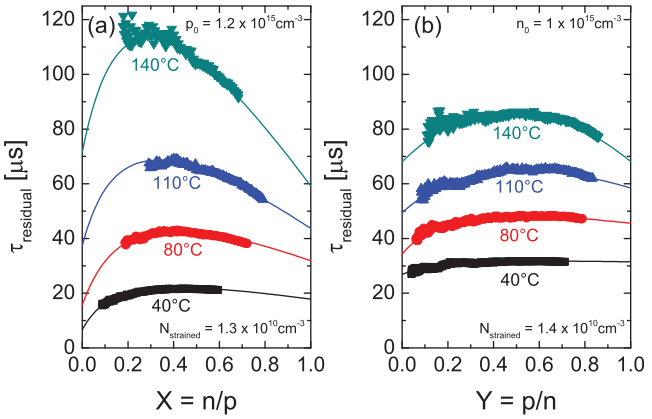

FIG. 9. Residual minority carrier lifetime versus (a) *n/p* for a p-type sample and (b) *p/n* for an n-type sample from Ingot 1. The experimental data have been fitted using two independent SRH centres.

of the two defects lie. The value of $Qn_1 + p_1$ (or $n_1 + \frac{p_1}{Q_1}$) obtained from Figure 6 indicate that the energy level of Defect 1 is at either $E_V + 0.22\,eV$ or $E_C - 0.25\,eV$. The value of $Q_2n_2 + p_2$ (or $n_2 + \frac{p_2}{Q_2}$) indicates the energy level of Defect 2 is at either $E_V + 0.26\,eV$ or $E_C - 0.08\,eV$. By comparing the temperature-dependence of the $Qn_1 + p_1$ with that of Qn_1 and p_1 given by Eqs. (2) and (3) with N_C and N_V taken as a function of temperature from Ref. 39, we deduce that Defect 1 is at $E_V + 0.22\,eV$. A similar approach for Defect 2 shows its energy level is at $E_C - 0.08\,eV$.

VI. DISCUSSION

A. Parameterisation of lifetime data

The linear formulation of SRH recombination described in Sec. II has provided an elegant framework by which to parameterise recombination at oxide precipitates and associated defects. Using this formulation, we have demonstrated that the recombination can be parameterised in terms of just two independent defects. Defect 1 has an energy level at $E_V + 0.22\,eV$ and a capture coefficient for electrons 157 times greater than that for holes at room temperature.

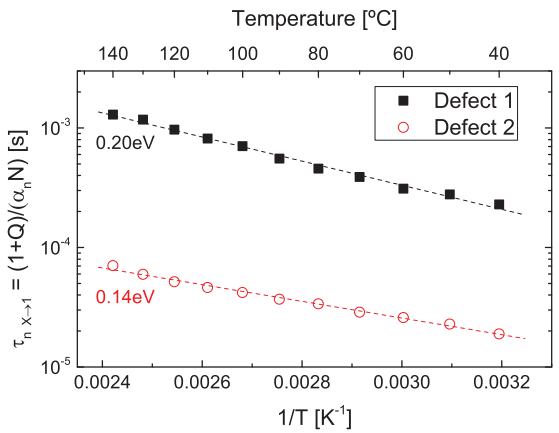

FIG. 10. The temperature-dependence of the X → 1 limit of the electron lifetime in p-type silicon containing oxide precipitates. Defect 1 has Q ≫ 1 so the activation energy of 0.20 eV is for α_{p1}. Defect 2 has Q ≪ 1 so the activation energy of 0.14 eV is for α_{n2}.

Defect 2 has an energy level at $E_C - 0.08\,eV$ and a capture coefficient for holes 1200 times greater than that for electrons at room temperature.

The minority carrier lifetime in both n-type and p-type samples increases with increasing temperature, as shown in Figures 2, 3 and 9. This supports the view that carriers are recombining at defects in the vicinity of the precipitates. An alternative process involving carrier capture by the precipitates would become more favourable with increased thermal activation and would therefore result in a reduction of lifetime with temperature. We have found that the capture coefficient for holes at Defect 1 (α_{p1}) decreases with temperature with a 0.20 eV activation energy. We have also found that the capture coefficient for electrons at Defect 2 (α_{n2}) decreases with temperature with a 0.14 eV activation energy. These activation energies seem reasonable when compared to other defects in silicon, which include 0.26 eV for holes at aluminium,[5] 0.11 eV for electrons at titanium,[40] 0.05 eV for electrons at cobalt,[41] and a hole cross-section which is independent of temperature at interstitial chromium.[42] In principle, the temperature dependences of the other two capture coefficients could be determined by performing variable-temperature measurements on samples with different doping levels, in accordance with Eq. (10). An alternative approach would be to make lifetime measurements at very low temperatures at which thermal emission is negligible.

Although the concentrations of the individual SRH defects cannot be determined by lifetime measurements alone, we have provided an empirical relation between the precipitate density and the recombination activity. Although the uncertainties in this are significant (a factor of two at best in the case of the dislocation-free precipitates), this parameterisation can be used empirically to quantify the effect of oxide precipitates on minority carrier lifetime in silicon. This is important as it means a relatively straightforward etching experiment can be used to place an upper limit on the minority carrier lifetime of the material.

B. Relative defect concentrations and presence of surrounding defects

TEM analysis has identified p-type samples in which some oxide precipitates are surrounded by other extended defects (dislocations and stacking faults). No additional levels are required to fit the injection-dependent lifetime curves measured for such samples, as the typical example in Figure 4(b) shows. Figure 7 shows the relationship between $N_1\alpha_{n1}$ and $N_2\alpha_{n2}$ and precipitate density is approximately linear. The linear relationship is only approximate which is to be expected given the large differences that occur between the structure of the precipitates and surrounding defects between samples. Figure 7 shows that $N_1\alpha_{n1}$ is an average factor of ~1.7 higher per precipitate and $N_2\alpha_{n2}$ is an average factor of ~2.9 higher per precipitate than for the samples in which no dislocations or stacking faults were found to surround the precipitates. Thus, it appears that other extended defects around the precipitates give rise to more of the same recombination-active defects that are associated with just the

precipitates themselves. We discuss possible defect structures in Sec. VI C.

C. Possible origins of the defects

There have been many studies into the electrical activity of defects in silicon containing oxide precipitates. DLTS studies have associated states with oxide precipitates at $E_V + 0.2\,eV$ to $E_V + 0.3\,eV$ (Refs. 20 and 43–45), $E_V + 0.4\,eV$ (Ref. 45), $E_C - 0.42\,eV$ to $E_C - 0.45\,eV$ (Refs. 20, 21, and 23), and $E_C - 0.22\,eV$ to $E_C - 0.25\,eV$ (Refs. 23 and 43). A shallower trap at approximately $E_C - 0.07\,eV$ was discovered in an electron beam induced current (EBIC) investigation.[22] The accuracy of determining energy levels from injection-dependent minority carrier lifetime measurements has been questioned in the literature.[3,5,41,46] However, the energy level we find for Defect 1 is consistent with one of the levels found by DLTS (Refs. 20 and 44–46) and the energy level for Defect 2 is consistent with that found by EBIC (Ref. 22). We do not find levels at $E_C - 0.22\,eV$ to $E_C - 0.25\,eV$. It is also noted that the traps at $E_V + 0.4\,eV$ (Ref. 45) and $E_C - 0.42\,eV$ to $E_C - 0.45\,eV$ (Refs. 20, 21, and 23) are "deep" in the sense that (for reasonable capture coefficients) the $\frac{p_1}{p_0}$ and $\frac{n_1}{n_0}$ terms in Eqs. (7) and (8) corresponding to them would be negligible at room temperature in samples with moderate doping levels. It is possible that recombination via these deeper traps would become measurable in our higher temperature measurements. There is no evidence for the existence of deep states in our p-type data temperature-dependent data (Figures 3 and 9(a)) nor in the relatively highly doped n-type data (Figures 2(a) and 9(b)). However, the low doped n-type data plotted in Figure 2(b) show a change in doping dependence above $\sim 90\,^{\circ}C$. It is possible that this could be explained in terms of recombination via one of the deeper states. However, the narrow *p*/*n* injection range of lifetime data for this sample means that it is not possible for us to determine any parameters accurately.

Clearly the precise physical origin of the defect states cannot be identified using injection-dependent lifetime measurements alone. Techniques such as EDMR and electron spin resonance (ESR) have shown recombination at oxide precipitates includes contribution from P_{b0} and P_{b1} dangling bonds.[25,47] Gerardi *et al.* found P_{b0} to have states at $E_V + 0.3\,eV$ and $E_V + 0.85\,eV$,[48] so the first of these could be associated with our Defect 2 and the second with our Defect 1. Levels associated with P_{b1} defects have been the matter of intense debate.[49–51] Recent results show that a P_{b1} level lies in the lower half of the band gap, closer to midgap than those due to P_{b0}.[51] We cannot confirm or deny the existence of this state, as, for reasons discussed above; it is unlikely that its effect on minority carrier lifetime would have been measurable given our range of temperatures and doping levels.

Oxide precipitates and associated dislocations and stacking faults are well-known to act as gettering centres for metallic impurities.[11,12] Even though the samples studied were processed in ultra-clean conditions, bulk iron concentrations of up to $4 \times 10^{11}\,cm^{-3}$ were measured in the p-type samples.[24] Low levels of impurity contamination are known strongly to affect the recombination properties of extended defects in silicon.[52,53] It is therefore possible that at least some levels found previously in DLTS and EBIC studies are impurity related. The fact that the presence of dislocations and stacking faults around the precipitates appears to increase the density of the *same* recombination centres could mean that at least some of the recombination activity is impurity related. That is, an impurity atom bound to an oxide precipitate may have the same SRH parameters as one bound to a dislocation or stacking fault. This topic is beyond the scope of this publication and is the subject of further investigation using intentionally contaminated samples.

The recombination rate has been found to be approximately dependent on the density of the precipitates, rather than their size. We have previously suggested recombination might occur at a feature of the precipitates which is invariant with their size, such as the corners of the strained platelets.[24,25] This could include a size-invariant feature at which impurity atoms are located. For the case in which no dislocations or stacking faults surround the precipitates in p-type material, the capture coefficient for electrons per precipitate is $1.7 \times 10^{-5}\,cm^3s^{-1}$ for Defect 1 and $1.8 \times 10^{-6}\,cm^3s^{-1}$ for Defect 2. Assuming each strained platelet has eight corners and that the thermal velocity of the carriers is $2 \times 10^7\,cm\,s^{-1}$, the respective capture cross-sections of the corner-related defects would be $\sigma_{n1} = 1.1 \times 10^{-13}\,cm^2$ and $\sigma_{n2} = 1.1 \times 10^{-14}\,cm^2$. These values are reasonable for defects in silicon.

VII. CONCLUSIONS

We have discussed a formulation of SRH statistics in which the lifetime is expressed in terms of the ratio of the total electron concentration to the total hole concentration for p-type (or vice versa for n-type) material. In this formulation, a single SRH defect manifests itself as a straight line on a plot of lifetime versus the ratio of the carrier concentrations. It has been shown how the gradient and limits at high and low injection can enable the SRH parameters to be extracted. This formulation is particularly elegant when multiple independent SRH defects operate, as injection-dependent lifetime can be fitted by combining straight lines in reciprocal. In a well-controlled sample set, injection-dependent minority carrier lifetime data can be analysed in terms of the SRH recombination to give the ratios of capture coefficients of electrons to those of holes and possible locations of energy levels. Such measurements do not enable absolute densities of the defects to be determined however.

Oxide precipitates are important defects in silicon for both integrated circuit and photovoltaic applications. Using the formulation of SRH statistics described above, we have been able to parameterise recombination due to oxide precipitates and associated defects. Injection-dependent lifetime data were acquired as a function of temperature from samples with different types, resistivities, and concentrations of strained precipitates. For most practical purposes in photovoltaics (i.e., low temperatures and moderate doping), the lifetime data can be modelled by the existence of just two independent defects. Defect 1 has a single energy level at $E_V + 0.22\,eV$ and has a capture coefficient for electrons 157 times greater than its capture coefficient for holes at room temperature. The capture

coefficient for holes at Defect 1 decreases with temperature with a 0.20 eV activation energy. Defect 2 has a single energy level at $E_C - 0.08$ eV and has a capture coefficient for holes 1200 times greater than its capture coefficient for electrons at room temperature. The capture coefficient for electrons at Defect 2 decreases with temperature with a 0.14 eV activation energy. Dislocations and stacking faults around the oxide precipitates increase the concentrations of the two defects, without introducing additional states into the bandgap. The role of impurities segregated to the oxide precipitates and surrounding defects requires further investigation.

ACKNOWLEDGMENTS

The authors are very grateful to D. Gambaro, M. Olmo, and M. Cornara at MEMC for performing the thermal treatments and precipitate density measurements, to staff at ISFH for surface passivation by remote PECVD, to R. Chakalova at Oxford for surface passivation by direct PECVD, and to V. Y. Resnik at the Institute of Rare Metals (Moscow) for performing TEM analysis. J.D.M. is the holder of a Royal Academy of Engineering/EPSRC Research Fellowship. The support of a Research Grant from the Royal Society is also acknowledged.

APPENDIX: RECOMBINATION AT A SINGLE DEFECT WITH TWO LEVELS

In this paper, it has been shown how plotting lifetime against n/p (for p-type) or p/n (for n-type) can allow SRH parameters to be deduced for independent single-level defects. In this Appendix, we show how the more complicated case of a single-defect with two levels would behave under this formulation of SRH statistics.

A single-defect with two levels has three possible states designated "State 0" in which no electrons have been captured, "State 1" in which one electron has been captured, and "State 2" in which two electrons have been captured. The concentrations of the states are designated m_0, m_1, and m_2 respectively. The energy level of State 1 is at E_1 and the energy level of State 2 is at E_2. The characteristic concentrations (given by Eqs. (2) and (3)) are p_1 and n_1 for State 1 and p_2 and n_2 for State 2. As in the single-level case, the kinetic equations for the state concentrations are those of the balance between capture and backward emission of the carriers

$$\frac{dm_0}{dt} = -\alpha_{n1}(nm_0 - n_1m_1) + \alpha_{p1}(pm_1 - p_1m_0) = 0, \quad \text{(A1)}$$

$$\frac{dm_2}{dt} = -\alpha_{p2}(pm_2 - p_2m_1) + \alpha_{n2}(nm_1 - n_2m_2) = 0, \quad \text{(A2)}$$

where the capture coefficients are α_{n1} for electrons by State 1, α_{p1} for holes by State 2, α_{n2} for electrons by State 2, and α_{p2} for holes by State 2.

By inspection of Eqs. (A1) and (A2), the recombination rate of electrons is

$$R = \alpha_{n1}(nm_0 - n_1m_1) + \alpha_{n2}(nm_1 - n_2m_2). \quad \text{(A3)}$$

There is an equivalent expression for holes. Equation (A3) can be re-arranged to give

$$R = m_1\left[\alpha_{n1}\left(n\frac{m_0}{m_1} - n_1\right) + \alpha_{n2}\left(n - n_2\frac{m_2}{m_1}\right)\right]. \quad \text{(A4)}$$

The three terms involving state concentrations in Eq. (A4) can instead be expressed in terms of capture coefficients and carrier concentrations. First, Eqs. (A1) and (A2) can be rearranged in terms of the ratio of state concentrations to give

$$\frac{m_0}{m_1} = \frac{\alpha_{n1}n_1 + \alpha_{p1}p}{\alpha_{n1}n + \alpha_{p1}p_1}, \quad \text{(A5)}$$

$$\frac{m_2}{m_1} = \frac{\alpha_{n2}n + \alpha_{p2}p_2}{\alpha_{n2}n_2 + \alpha_{p2}p}. \quad \text{(A6)}$$

Second, the defect concentration, M, is equal to the sum of m_0, m_1, and m_2, so we can write

$$m_1 = \frac{M}{1 + \frac{m_0}{m_1} + \frac{m_2}{m_1}}. \quad \text{(A7)}$$

Substituting Eqs. (A5)–(A7) into Eq. (A4) gives

$$R = \frac{M}{1 + \left(\frac{\alpha_{n1}n_1 + \alpha_{p1}p}{\alpha_{n1}n + \alpha_{p1}p_1}\right) + \left(\frac{\alpha_{n2}n + \alpha_{p2}p_2}{\alpha_{n2}n_2 + \alpha_{p2}p}\right)} \cdot \left[\alpha_{n1}\left(\frac{\alpha_{p1}np - \alpha_{p1}n_1p_1}{\alpha_{n1}n + \alpha_{p1}p_1}\right) + \alpha_{n2}\left(\frac{\alpha_{p2}np - \alpha_{p2}n_2p_2}{\alpha_{n2}n_2 + \alpha_{p2}p}\right)\right]. \quad \text{(A8)}$$

The n_1p_1 and n_2p_2 products are equal to n_i^2 and can be safely neglected compared to the np product terms and the relatively low temperatures at which injection-dependent lifetime measurements are made. Equation (A8) therefore becomes

$$R = \frac{\mathrm{Mnp}}{1 + \left(\frac{\alpha_{n1}n_1 + \alpha_{p1}p}{\alpha_{n1}n + \alpha_{p1}p_1}\right) + \left(\frac{\alpha_{n2}n + \alpha_{p2}p_2}{\alpha_{n2}n_2 + \alpha_{p2}p}\right)} \times \left[\left(\frac{\alpha_{n1}\alpha_{p1}}{\alpha_{n1}n + \alpha_{p1}p_1}\right) + \left(\frac{\alpha_{n2}\alpha_{p2}}{\alpha_{n2}n_2 + \alpha_{p2}p}\right)\right]. \quad \text{(A9)}$$

Equation (A9) is universal and applies to both p-type and n-type. The electron lifetime in p-type material, τ_n, is given by $\tau_n = \frac{\Delta n}{R}$. Equation (A9) can be written in terms of $X = \frac{n}{p}$ using Eq. (6) to give

$$\tau_n = \frac{1 + \left(\frac{\frac{Q_1n_1(1-X)}{p_0} + 1}{Q_1X + \frac{p_1(1-X)}{p_0}}\right) + \left(\frac{X + \frac{p_2(1-X)}{Q_2p_0}}{\frac{n_2(1-X)}{p_0} + \frac{1}{Q_2}}\right)}{M\left[\frac{\alpha_{n1}}{Q_1X + \frac{p_1(1-X)}{p_0}} + \frac{\alpha_{p2}}{\frac{n_2(1-X)}{p_0} + \frac{1}{Q_2}}\right]}, \quad \text{(A10)}$$

where $Q_1 = \frac{\alpha_{n1}}{\alpha_{p1}}$ and $Q_2 = \frac{\alpha_{n2}}{\alpha_{p2}}$.

It can also be shown that the lifetime of holes in n-type material varies with $Y = \frac{p}{n}$ according to

$$\tau_p = \frac{1 + \left(\frac{\left(\frac{Q_1 n_1 (1-Y)}{n_0}\right) + Y}{Q_1 + \frac{p_1(1-Y)}{n_0}}\right) + \left(\frac{1 + \frac{p_2(1-Y)}{Q_2 n_0}}{\frac{n_2(1-Y)}{n_0} + \frac{Y}{Q_2}}\right)}{M\left[\frac{\alpha_{n1}}{Q_1 + \frac{p_1(1-Y)}{n_0}} + \frac{\alpha_{p2}}{\frac{n_2(1-Y)}{n_0} + \frac{Y}{Q_2}}\right]}. \tag{A11}$$

Equations (A10) and (A11) simplify when the first level is in the lower half of the gap and the second level is in the upper half. In this scenario, n_1 and p_2 are negligible and thermal emission is represented only by p_1 (hole emission leading to the transition from State 0 to State 1) and n_2 (electron emission leading to the transition from State 2 to State 1).

[1] R. N. Hall, Phys. Rev. **87**, 387 (1952).
[2] W. Shockley and W. T. Read, Phys. Rev. **87**, 835 (1952).
[3] S. Rein, T. Rehrl, W. Warta, and S. W. Glunz, J. Appl. Phys. **91**, 2059 (2002).
[4] D. Macdonald and A. Cuevas, Phys. Rev. B **67**, 075203 (2003).
[5] J. Schmidt, Appl. Phys. Lett. **82**, 2178 (2003).
[6] R. Falster and G. Borionetti, "Recombination lifetime measurements in silicon," ASTM STP **1340**, 226 (1998).
[7] R. A. Sinton and A. Cuevas, Appl. Phys. Lett. **69**, 2510 (1996).
[8] D. V. Lang, J. Appl. Phys. **45**, 3023 (1974).
[9] K. Bothe, K. Ramspeck, D. Hinken, C. Schinke, J. Schmidt, S. Herlufsen, R. Brendel, J. Bauer, J.-M. Wagner, N. Zakharov, and O. Breitenstein, J. Appl. Phys. **106**, 104510 (2009).
[10] J. Haunschild, I. E. Reis, J. Geilker, and S. Rein, Phys. Status Solidi (RRL) **5**, 199 (2011).
[11] R. Falster and W. Bergholz, J. Electrochem. Soc. **137**, 1548 (1990).
[12] D. Gilles, E. R. Weber, and S. K. Hahn, Phys. Rev. Lett. **64**, 196 (1990).
[13] M. Syre, S. Karazhanov, B. R. Olaisen, A. Holt, and B. G. Svensson, J. Appl. Phys. **110**, 024912 (2011).
[14] K. Jurkschat, S. Senkader, P. R. Wilshaw, D. Gambaro, and R. J. Falster, J. Appl. Phys. **90**, 3219 (2001).
[15] Z. Zeng, J. Chen, Y. Zeng, X. Ma, and D. Yang, J. Cryst. Growth **324**, 93 (2011).
[16] P. K. Kulshreshtha, YoHan Yoon, K. M. Youssef, E. A. Good, and G. Rozgonyi, J. Electrochem. Soc. **159**, H125 (2012).
[17] K. H. Yang, H. F. Kappert, and G. H. Schwuttke, Phys. Status Solidi A **50**, 221 (1978).
[18] M. Miyagi, K. Wada, J. Osaka, and N. Inoue, Appl. Phys. Lett. **40**, 719 (1982).
[19] S. S. Chan, C. J. Varker, J. D. Whitfield, and R. W. Carpenter, Mater. Res. Soc. Symp. Proc. **46**, 281 (1985).
[20] J. M. Hwang and D. K. Schroder, J. Appl. Phys. **59**, 2476 (1986).
[21] J. Vanhellemont, E. Simoen, A. Kaniava, M. Libezny, and C. Claeys, J. Appl. Phys. **77**, 5669 (1995).
[22] W. Seifert, M. Kittler, and J. Vanhellemont, Mater. Sci. Eng. B **42**, 260 (1996).
[23] T. Mchedlidze, K. Matsumoto, and E. Asano, Jpn. J. Appl. Phys., Part 1 **38**, 3426 (1999).
[24] J. D. Murphy, K. Bothe, M. Olmo, V. V. Voronkov, and R. J. Falster, J. Appl. Phys. **110**, 053713 (2011).
[25] V. Lang, J. D. Murphy, R. J. Falster, and J. J. L. Morton, J. Appl. Phys. **111**, 013710 (2012).
[26] L. Chen, X. Yu, P. Chen, P. Wang, X. Gu, J. Lu, and D. Yang, Sol. Energy Mater. Sol. Cells **95**, 3148 (2011).
[27] W. Bergholz, M. J. Binns, G. R. Booker, J. C. Hutchison, S. H. Kinder, S. Messoloras, R. C. Newman, R. J. Stewart, and J. G. Wilkes, Philos. Mag. B **59**, 499 (1989).
[28] R. Falster, V. V. Voronkov, V. Y. Resnik, and M. G. Milvidskii, in *Proceedings of the Electrochemical Society, High Purity Silicon VIII* (Electrochemical Society, Pennington, NJ, USA, 2004), Vol. 200405, p. 188.
[29] V. V. Voronkov, R. Falster, J. Schmidt, K. Bothe, and A. V. Batunina, ECS Trans. **33**, 103 (2010).
[30] V. V. Voronkov, R. Falster, K. Bothe, B. Lim, and J. Schmidt, J. Appl. Phys. **110**, 063515 (2011).
[31] K. F. Kelton, R. Falster, D. Gambaro, M. Olmo, M. Cornara, and P. F. Wei, J. Appl. Phys. **85**, 8097 (1999).
[32] T. Lauinger, J. Moschner, A. G. Aberle, and R. Hezel, J. Vac. Sci. Technol. A **16**, 530 (1998).
[33] K. Bothe and J. Schmidt, J. Appl. Phys. **99**, 013701 (2006).
[34] G. Zoth and W. Bergholz, J. Appl. Phys. **67**, 6764 (1990).
[35] S. Rein and S. W. Glunz, J. Appl. Phys. **98**, 113711 (2005).
[36] J. D. Murphy and R. J. Falster, Phys. Status Solidi (RRL) **5**, 370 (2011).
[37] H. Schlangenotto, H. Maeder, and W. Gerlach, Phys. Status Solidi A **21**, 357 (1974).
[38] M. J. Kerr and A. Cuevas, J. Appl. Phys. **91**, 2473 (2002).
[39] M. A. Green, J. Appl. Phys. **67**, 2944 (1990).
[40] B. B. Paudyal, K. R. McIntosh, and D. H. Macdonald, J. Appl. Phys. **105**, 124510 (2009).
[41] S. Diez, S. Rein, T. Roth, and S. W. Glunz, J. Appl. Phys. **101**, 033710 (2007).
[42] J. Schmidt, R. Krain, K. Bothe, G. Pensl, and S. Beljakowa, J. Appl. Phys. **102**, 123701 (2007).
[43] M. Koizuka and H. Yamada-Kaneta, J. Appl. Phys. **84**, 4255 (1998).
[44] K. Mallik, R. J. Falster, and P. R. Wilshaw, Solid-State Electron. **48**, 231 (2004).
[45] B. Pivac, S. Ilíc, A. Borghesi, A. Sassella, and M. Porrini, Vacuum **71**, 141 (2003).
[46] B. B. Paudyal, K. R. McIntosh, D. H. Macdonald, and G. Coletti, J. Appl. Phys. **107**, 054511 (2010).
[47] M. Koizuka and H. Yamada-Kaneta, J. Appl. Phys. **88**, 1784 (2000).
[48] G. J. Gerardi, E. H. Poindexter, P. J. Caplan, and N. M. Johnson, Appl. Phys. Lett. **49**, 348 (1986).
[49] A. Stesmans and V. V. Afanas'ev, Appl. Phys. Lett. **78**, 1451 (2001).
[50] J. P. Campbell and P. M. Lenahan, Appl. Phys. Lett. **80**, 1945 (2002).
[51] L. Dobaczewski, S. Bernardini, P. Kruszewski, P. K. Hurley, V. P. Markevich, I. D. Hawkins, and A. R. Peaker, Appl. Phys. Lett. **92**, 242104 (2008).
[52] T. S. Fell, P. R. Wilshaw, and M. D. de Coteau, Phys. Status Solidi A **138**, 695 (1993).
[53] V. Kveder, M. Kittler, and W. Schröter, Phys. Rev. B **63**, 115208 (2001).